Materials Advances

ROYAL SOCIETY OF CHEMISTRY

PAPER

View Article Online
View Journal | View Issue



Cite this: *Mater. Adv.*, 2025, 6, 5232

# Tailoring poly(vinylbenzocyclobutene)-*b*-poly(4-vinylpyridine) isoporous block copolymer membranes: functionalization and performance optimization†

Michael Appold, Sofia Rangou, * Brigitte Lademann and Volkan Filiz *

Received 19th February 2025,
Accepted 9th June 2025

DOI: 10.1039/d5ma00157a

rsc.li/materials-advances

Amphiphilic block copolymers are promising candidates for the fabrication of ultrafiltration membranes with an isoporous integral asymmetric structure. Within this study we demonstrate the synthesis and membrane fabrication of the new block copolymer (BCP) poly(vinylbenzocyclobutene)-*b*-poly(4-vinylpyridine) (PVBCB-*b*-P4VP). The membranes were fabricated using a self-assembly non-solvent induced phase separation process (SNIPS) resulting in an isoporous integral asymmetric structure comprising a unique foam-like substructure with a homogenous three-dimensional porosity throughout the whole membrane body. The dependence of the membrane formation process on the evaporation time, the polymer concentration of the initial casting solution and the molecular weight as well as the block copolymer composition was investigated. Furthermore, the pore diameters of the BCP membranes were tailor-made by simply adjusting the molecular weight of the pore forming P4VP block segments. Moreover, the BCP membranes were functionalized with octylbromide resulting in quaternized P4VP block segments and consequently in positively charged pores. Finally, water flux and retention measurements with proteins of the pristine and functionalized membranes were demonstrated.



## Introduction

Membrane technology has revolutionized various industries, ranging from water treatment to biomedical engineering, by enabling efficient separation processes with minimal energy consumption. Key to the success of membrane-based systems is the meticulous design of membrane materials, where the properties of the constituent polymers play a pivotal role. Among these materials, amphiphilic block copolymers have garnered significant attention due to their ability to self-assemble into well-defined nanostructures, offering unparalleled versatility in membrane design.[1]

The modification of amphiphilic block copolymers has profound implications for membrane performance across diverse applications.[2] In water treatment, tailored membranes exhibit enhanced fouling resistance, improved permeability, and selective separation capabilities, addressing critical challenges in desalination, wastewater treatment, and purification processes. In biomedical applications, modified membranes offer precise control over drug delivery kinetics, cellular interactions, and tissue regeneration, opening new avenues for personalized medicine and regenerative therapies.[3–5] Furthermore, the versatility of modified membranes extends to energy-related applications, including gas separation, fuel cells, and energy storage devices, where tailored properties enhance efficiency and sustainability.[6,7]

Amphiphilic block copolymers consist of distinct hydrophilic and hydrophobic segments, which spontaneously organize into ordered nanostructures in solution.[8,9] The interplay between polymer–polymer and polymer–solvent interactions drives the self-assembly process, resulting in the formation of various morphologies, such as micelles, vesicles, and lamellar structures.[10,11] Understanding the intricate balance of forces governing copolymer self-assembly is essential for rational design and modification of membrane materials. Modifying one branch of amphiphilic block copolymers offers a powerful means of tailoring membrane properties while retaining the inherent advantages of the parent polymer.[10] Various modification strategies have been developed, including chemical functionalization, polymer blending, and surface grafting techniques. These approaches enable precise control over membrane morphology, pore size, surface chemistry, and mechanical properties, thereby optimizing performance for specific applications.[9,12,13] Moreover, modification at the molecular level facilitates the incorporation of functional groups or stimuli-responsive moieties, imparting advanced functionalities such as selective permeability,

*Helmholtz-Zentrum hereon, Institute of Membrane Research, Max-Planck-Straße 1, 21502, Geesthacht, Germany. E-mail: volkan.filiz@hereon.de, sofia.rangou@hereon.de; Tel: +49 4152 872425, +49 4152 872498*

† Electronic supplementary information (ESI) available. See DOI: https://doi.org/10.1039/d5ma00157a

antimicrobial activity, and responsiveness to external stimuli.[9,14–19]

This article explores the transformative potential of modifying one branch of amphiphilic block copolymers, paving the way for tailored membranes with enhanced performance and functionality.

# Experimental

### Reagents

All solvents and reagents were purchased from Alfa Aesar, Sigma Aldrich, Fisher Scientific, ABCR and used as received unless otherwise stated. Tetrahydrofuran (THF) was distilled from sodium/benzophenone under reduced pressure (cryo-transfer) prior to the addition of 1,1-diphenylethylene and *n*-butyllithium (*n*-BuLi) followed by a second cryo-transfer. Vinylbenzocyclobutene (VBCB) (Sigma-Aldrich) was dried over calcium hydride and distilled twice from di-*n*-butylmagnesium *via* cryo-transfer. 4-Vinylpyridine (4VP) (Sigma-Aldrich) was first distilled from calcium hydride and afterwards cryo-transferred from ethyl aluminium dichloride prior to use in polymerization. All polymerization reactions were carried out in a Schlenk line apparatus using high vacuum ($10^{-7}$–$10^{-8}$ mbar) and argon (Argon 7.0, Linde AG).

### Instrumentation

NMR spectra were recorded on a Bruker Ascend 500 NMR spectrometer working at 500 MHz ($^1$H NMR) using CDCl3 and DMF-d7 as solvents at room temperature. NMR chemical shifts are referenced relative to tetramethylsilane (TMS). Standard SEC was performed using a system composed of a VWR-Hitachi 2130 pump and a Shodex RI-101 refractive index detector at 30 °C, $CHCl_3$ as the mobile phase (flow rate 1 mL min$^{-1}$) on a GRAM column set from PSS (GRAM precolumn (dimension 8·50 mm), GRAM column (porosity 3000 A, dimension 8·300 mm, particle size 10 μm) and GRAM column (porosity1000 A, dimension 8·300 mm, particle size 10 μm). Calibration was carried out using PS standards (from Polymer Standard Service, Mainz). For data acquisition and evaluation of the measurements, PSS WinGPC® UniChrom 8.2 was used. SEM measurements were performed on a LEO Gemini 1550 VP (Zeiss, Oberkochen, Germany) at an operating voltage of 3–5 kV using secondary electron detector. Prior to SEM measurements the polymer samples were coated with 2 nm platinum using a sputter coater. Cross-sections of the membranes were prepared while dipping the membranes in isopropanol, freezing in liquid nitrogen, and breaking. Average pore size values were determined using the software analysis (Olympus Soft Imaging Solutions GmbH, Münster, Germany) on the basis of the SEM results. Water flux and retention measurements were performed using a stirred test cell (EMD Millipore™ XFUF04701) (Merck Millipore, Darmstadt, Germany) in dead-end mode at a trans-membrane pressure (TMP) of 2 bar at room temperature. The membrane area was 1.8 cm$^2$. These studies were conducted employing demineralized water with an electrical conductivity of ≈0.055 μS cm$^{-1}$. BSA (bovine serum albumin) (Sigma-Aldrich, Schnelldorf, Germany) dissolved in PBS buffer solution at a concentration of 1 g L$^{-1}$ and haemoglobin solutions with a concentration of 1 g L$^{-1}$ in a PBS buffer solution (10 mM PBS, 0.9 wt% NaCl) (Sigma-Aldrich, Schnelldorf, Germany) were employed for the retention measurements. For determination of the thermal properties of the polymers differential scanning calorimetry (DSC) was performed with a Mettler Toledo DSC-1 in a temperature range from −100 °C to 150 °C with a heating rate of 10 K min$^{-1}$.

### Anionic polymerization of vinylbenzocyclobutene and 4-vinylpyridine

Exemplary synthesis of a poly(vinylbenzocyclobutene-*block*-4-vinylpyridine) featuring a molar mass of 109 kg mol$^{-1}$ ($PVBCB_{79}$-*b*-$P4VP_{21}^{109k}$).

In a 250 mL glass reactor equipped with a stirring bar, subsequently purified THF was distilled and titrated under argon by a small amount of *s*-BuLi until a vivid yellow colour was observed. Upon the disappearance of the colour the reactor was brought to −80 °C and 2.213 g (0.023 mol, 1045 eq.) of purified 4-vinylbenzocyclobutene was added to the reactor. The polymerization was initiated by quick addition of 0.08 mL *s*-BuLi (0.000022 mol, 1 eq., 0.28 M solution in cyclohexane) with a syringe. The solution was stirred for 1 hour at −80 °C to ensure complete conversion of 4-vinylbenzocyclobutene before an aliquot of the solution was taken from the reactor for characterization of the PVBCB segment and terminated with methanol. Afterwards 0.539 g (0.0056 mmol, 255 eq.) purified 4-vinylpyridine was added to the solution and stirred for an additional 24 hours. After adding a small amount of degassed methanol, the polymer was precipitated in a 10-fold excess of hexane. The polymer was collected by filtration, washed with hexane and dried in a vacuum (yield: 2.75 g, 96%).

SEC (*vs.* PS): PVBCB: $M_n$ = 85 900 g mol$^{-1}$; $M_w$ = 88 500 g mol$^{-1}$; $Đ$ = 1.03.

PVBCB-*b*-P4VP: $M_n$ = 85 600 g mol$^{-1}$; $M_w$ = 89 700 g mol$^{-1}$; $Đ$ = 1.05.

$^1$H-NMR (500 MHz, 300 K, $CDCl_3$, $\delta$ in ppm): 7.18–6.91 (br, H4/5), 6.78–6.33 (br, H3), 3.60 (br, H8), 2.24–0.83 (alkyl).

### Membrane fabrication of PVBCB-*b*-P4VP BCP's using the SNIPS process

The block copolymer $PVBCB_{79}P4VP_{21}^{109k}$ is dissolved in a mixture of dimethylformamide (DMF), dioxane (DIOX) and tetrahydrofuran (THF) to provide a viscus but clear casting solution. The composition of the casting solution is 20 wt% PVBCB-*b*-P4VP, 36 wt% THF, 36 wt% DIOX and 8 wt% DMF. The casting solution is spread out using a home-made casting machine using a doctor blade with a gap height adjusted to 200 μm on a polyester nonwoven support. After 10 seconds, the film is immersed in a water bath. Drying of the membrane follows at 60 °C under vacuum.

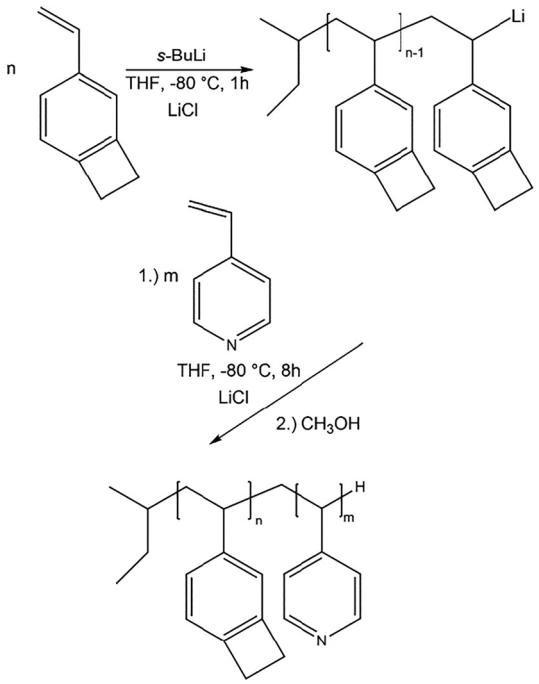


Scheme 1 Sequential anionic block copolymerization of 4-vinylbenzocyclobutene (VBCB) and 4-vinylpyridine (4VP) in THF in the presence of LiCl at −80 °C to yield PVBCB-*b*-P4VP block copolymers.

### Functionalization of PVBCB-*b*-P4VP block copolymer membranes

A membrane disc with a diameter of 2 cm was placed in a three-necked 250 mL glass reactor and 50 mL ethanol were added. After the mixture was heated to reflux 0.2 mL octylbromide were added, and the membrane was functionalized for 24 hours under reflux. Afterwards the membrane was washed with ethanol and dried at 60 °C under vacuum.

## Results and discussion

The aim of the corresponding work was the development and optimization of the hexagonally packed pore structures on membrane surfaces from amphiphilic block copolymers. The membranes were fabricated *via* the well-known SNIPS process by varying the molecular weights and compositions of the block copolymers as well as the casting conditions like concentration and evaporation time. For PS-*b*-P4VP block copolymers the membrane formation processes with all parameters is well studied, which is why we are focusing on new PVBCB-*b*-P4VP block copolymers in this work. In contrast to former block copolymer membranes the PVBCB segments pave the way for thermal and chemical stable ultrafiltration membranes by UV cross-linking of the cyclobutene moieties, which is the focus of an upcoming study.

### Characterization of PVBCB-*b*-P4VP block copolymers

For the fabrication of isoporous integral asymmetric ultrafiltration membranes with hexagonally ordered pores on the surface, block copolymers with defined molecular weights and compositions are basic prerequisites. Therefore, block copolymers consisting of 4-polyvinylbenzocyclobutene (PVBCB) as the matrix building block and poly(4-vinylpyridine) (P4VP) as a second cylinder forming block segment were prepared. PVBCB-*b*-P4VP block copolymers were synthesized *via* sequential anionic polymerization in THF starting from 4-vinylbenzocyclobutene (VBCB) with *sec*-butyllithium (*s*-BuLi) as the initiator at −80 °C as shown in Scheme 1. After stirring for one hour 4-vinylpyridine (4VP) was added for the preparation of the second block segment. The reaction was terminated after additional stirring of 24 hours at −80 °C by the addition of degassed methanol.

The corresponding PVBCB-*b*-P4VP block copolymers were characterized with respect to their molecular weights and compositions using size exclusion chromatography (SEC) and $^1$H NMR spectroscopy (Fig. S7, ESI†). All obtained data comprising $M_n$, $M_w$ and dispersity index values, $Đ$, for the investigated PVBCB precursors and the corresponding PVBCB-*b*-P4VP block copolymers within this study are compiled in Table 1. For better comparison the polymer samples were classified by subscripts indicating the weight percentage of each block in the polymer and the number following is attributed to the total molecular weight in kg mol$^{-1}$.

The block copolymer overall molecular weights are in the range of 105.000 g mol$^{-1}$ to 138.000 g mol$^{-1}$ with P4VP

Table 1 Molecular weights, dispersity indices and composition in weight percentage of all block copolymers synthesized in this study

| Polymer | $M_n$[a] (kg mol$^{-1}$) | $M_w$[a] (kg mol$^{-1}$) | $Đ$[a] | $M_n$[b] (kg mol$^{-1}$) | wt% PVBCB/P4VP |
|---|---|---|---|---|---|
| PVBCB$^{84k}$ | 84 | 89 | 1.05 | — | — |
| PVBCB$_{80}$-*b*-P4VP$_{20}^{105k}$ | 88 | 97 | 1.09 | 105 | 80/20 |
| PVBCB$^{86k}$ | 86 | 89 | 1.03 | — | — |
| PVBCB$_{79}$-*b*-P4VP$_{21}^{109k}$ | 86 | 89 | 1.05 | 109 | 79/21 |
| PVBCB$^{92k}$ | 90.5 | 95 | 1.05 | — | — |
| PVBCB$_{81}$-*b*-P4VP$_{19}^{113k}$ | 122 | 129 | 1.06 | 113 | 81/19 |
| PVBCB$^{93k}$ | 92 | 97 | 1.05 | — | — |
| PVBCB$_{79}$-*b*-P4VP$_{21}^{118k}$ | 98 | 108 | 1.10 | 118 | 79/21 |
| PVBCB$^{110k}$ | 110 | 115 | 1.05 | — | — |
| PVBCB$_{80}$-*b*-P4VP$_{20}^{138k}$ | 113 | 118 | 1.04 | 138 | 80/20 |

[a] Molecular weight determined by SEC (PS standards, $CHCl_3$). [b] Molecular weight determined by combination of SEC measurements and $^1$H-NMR spectroscopy.

compositions from 19 wt% to 21 wt%. Good control over the anionic polymerization was evidenced as indicated by narrow molecular weight distributions with dispersity index values $Đ$ in the range of 1.04–1.10 for the PVBCB-*b*-P4VP block copolymers.

The molar mass distributions of all PVBCB precursors und PVBCB-*b*-P4VP block copolymers after sequential anionic polymerization were obtained by SEC in $CHCl_3$ *vs.* PS standards (Fig. S3–S7, ESI†). All molecular weight distributions for the PVBCB-*b*-P4VP block copolymers (left images corresponding images Fig. S3–S7, ESI†) are shifted towards higher molar masses compared to the corresponding PVBCB precursors (right images in the corresponding images Fig. S3–S7, ESI†). This fact proves the successful BCP formation without significant termination of the PVBCB precursors acting as anionic macro initiators. Additionally, the overall molecular weights and the composition of the block copolymers used in this study were calculated from the corresponding $^1$H NMR spectra at the signal area of 6.2–7.2 ppm from PVBCB and at 8.2 ppm for P4VP. The calculated molecular weights and weight percentages of the PVBCB and P4VP block segments are additionally given in Table 1. Overall molar masses determined by SEC and by calculation from SEC and NMR spectroscopy show slightly different values. This can be explained by the fact that SEC is a relative method with PS as standards and hydrodynamic radii for the amphiphilic PVBCB-*b*-P4VP block copolymers, especially for the P4VP segments, differ compared to PS homopolymers.

The thermal properties of the block copolymers were investigated by differential scanning calorimetry (DSC) measurements (Fig. S11, ESI†). DSC measurements for all block copolymers used in this work revealed one visible glass transition temperature at 125 °C, which can be assigned to the PVBCB block segments. A second glass transition temperature is indicated at around 145 °C and can be assigned to the P4VP block segments. However, this second glass transition temperature is weakly pronounced due to a very strong exothermic peak starting at 180 °C and showing a maximum at 280 °C. This strong exothermic peak can be assigned to the thermal cross-linking reaction of the PVBCB block segments. During the heating process, the benzocyclobutene moieties can transform into *o*-xylene units. This very reactive species readily undergo inter- and intramolecular cyclo-reactions like Diels–Alder reaction to produce polycyclic compounds with high stability, such as cyclooctadiene (Fig. S1, ESI†). The polymerization of *o*-quinodimethane is like that of 1,3-dienes resulting in linear polymers.

In summary, DSC and SEC measurements proved – together with the $^1$H NMR spectra featuring all characteristic signals for PVBCB and P4VP – the successful formation of the amphiphilic PVBCB-*b*-P4VP block copolymers by sequential anionic polymerization. The fabrication of the block copolymer membranes by SNIPS process will be shown in the next section followed by a detailed study about the surface structure of the corresponding membranes.

### Membrane formation using the SNIPS process

In general, ultrafiltration membranes can be fabricated from block copolymers by the so-called self-assembly non-solvent induced phase separation (SNIPS) process combining the self-assembly of block copolymers with the well-established non-solvent induced phase separation (NIPS) process. This membrane formation procedure can be divided into the following two steps: (i) due to evaporation of the solvent microphase separation of the block copolymers to micelles occurs, followed by self-assembly of these micelles driven by the increasing concentration gradient in the solution. (ii) Freezing and fixation of the surface structure by precipitation of the block copolymers. During this step, the solvent of the swollen polymers is replaced by the non-solvent water resulting in isoporous integral asymmetric membranes with hexagonally ordered pores on the surface. During the membrane fabrication process, five key parameters are crucial for the surface structure: (i) overall molecular weight of the block copolymers, (ii) polymer composition of the different block segments, (iii) the solvent mixture and (iv) block copolymer concentration in the solution as well as (v) the evaporation time prior to precipitation. As the evaporation time strongly influences the self-assembly of the block copolymer and thus the surface structure of the resulting membrane, the membrane formation process was realized on an automated custom-made casting machine (Fig. S2, ESI†).

From PS-*b*-P4VP block copolymer membranes it is well known that a ternary mixture from DMF/THF/DIOX provides the best results for the isoporous surface structure. Based on these reported results we chose a fixed solvent mixture of DMF/THF/DIOX with a ratio of 10/45/45 wt% for all casting experiments. In this case, THF and dioxane are more selective for the PVBCB block segments while DMF is selective for P4VP. The P4VP chains tend to precipitate in THF and dioxane for which reason block copolymers can self-assemble to form micelles in the casting solution. After casting of the block copolymer solution, the more volatile THF starts to evaporate resulting in micelle formation or self-assembly of the existing micelles due to the increasing polymer concentration on the surface. At the same time, the matrix building PVBCB block segments start to precipitate, while the core forming P4VP segments are swollen with DMF. Afterwards the casted solution is immersed into a water bath, where the membrane is completely precipitated, and the surface structure is frozen. During this step, DMF of the swollen P4VP domains is replaced by water leading to a collapse of the P4VP chains and resulting in open cylindrical hexagonally ordered pores on the surface. Due to the concentration gradient in the casting solution, ranging from being concentrated on the top and decreasing to the bottom, the

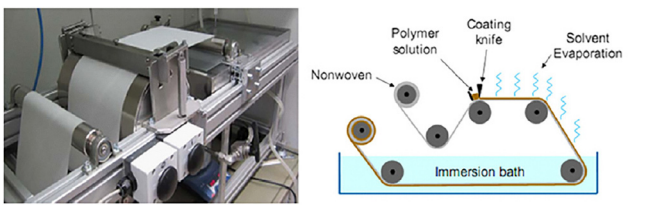


Fig. 1 Photo of laboratory-size casting machine (left) and schematic presentation of the casting process (right) (reprinted with permission from ref. 9).

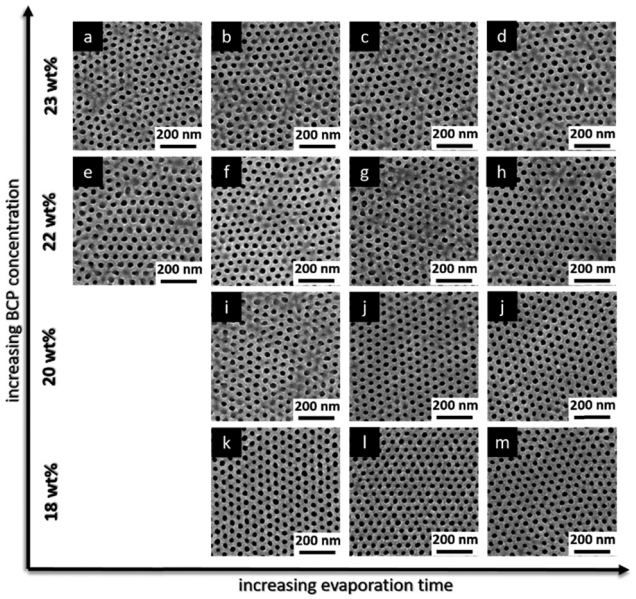


Fig. 2 SEM images of the membrane surfaces casted from PVBCB$_{80}$-*b*-P4VP$_{20}^{105k}$ block copolymers. (a)–(d) Membranes were cast from 23 wt% block copolymer solutions in DMF/THF/DIOX – 10/45/45 with varying evaporation times between 9 and 14 s. (e)–(h) Membranes were cast from 22 wt% block copolymer solutions in DMF/THF/DIOX – 10/45/45 with varying evaporation times between 9 and 17 s. (i) and (j) Membranes were cast from 20 wt% block copolymer solutions in DMF/THF/DIOX – 10/45/45 with varying evaporation times between 12 and 20 s. (k)–(m) Membranes were cast from 18 wt% block copolymer solutions in DMF/THF/DIOX– 10/45/45 with varying evaporation times between 12 and 20 s.

membrane shows a porous sponge-like substructure, resulting in an integral asymmetric membrane (Fig. 1).

To get a deeper understanding of the membrane formation process generating integral asymmetric membranes with perfect hexagonally ordered pores on the surface of new PVBCB-*b*-P4VP block copolymers, different experiments with varying polymer concentrations in the initial casting solution and evaporation times were conducted. In Fig. 2 the plot of the membrane surface structure of block copolymer PVBCB$_{80}$-*b*-P4VP$_{20}^{105k}$ with different polymer concentrations in the casting solution *versus* the evaporation time is shown.

As can be seen in Fig. 2 it was possible to fabricate PVBCB$_{80}$-*b*-P4VP$_{20}^{105k}$ block copolymer membranes with ordered surface structures at polymer concentrations in the range of 18 to 23 wt% of the initial casting solution. In general, no polymer sample we used in our study showed an open pore structure with polymer concentrations of more than 24 wt%. The best membrane structures were observed at polymer concentrations of 18 and 20 wt% with long evaporation times. With decreasing evaporation time prior to precipitation form and size of the pores were getting more irregular. By further increasing the polymer concentration the viscosity of the casting solution also increases, resulting in faster precipitation of the matrix building PVBCB chains. Consequently, the required density on the membrane surface is reached faster and the evaporation time has to be decreased to obtain a good surface structure. Nevertheless, the surface structure is getting more irregular when increasing the polymer concentration over 20 wt% independent of the evaporation time. As can be concluded from Fig. 2 there is a strong dependency of the order of the pores on the polymer concentration and the evaporation time prior to precipitation.

Apart from the influence of the polymer concentration and the evaporation time, the effect of the molecular weight on the structure formation process was also further investigated. For this purpose, a series of experiments were carried out where the molecular weight was systematically increased while the P4VP content was nearly constant. In Fig. 3 the membrane surface structure of PVBCB-*b*-P4VP block copolymers with different molecular weights depending on the polymer concentration in the initial casting solution is shown. The molecular weight of the block copolymers was increased from 105 kg mol$^{-1}$ over 113 kg mol$^{-1}$ up to 138 kg mol$^{-1}$ while the P4VP content was with 19 and 20 wt% nearly constant. The polymer concentration in the casting solution was varied from 14 to 18 wt% for PVBCB$_{80}$-*b*-P4VP$_{20}^{138k}$, from 17 to 22 wt% for PVBCB$_{81}$-*b*-P4VP$_{19}^{113k}$ and from 18 to 24 wt% for PVBCB$_{80}$-*b*-P4VP$_{20}^{105k}$ block copolymers. All parameters used for the SNIPS process of the membranes shown in Fig. 3 are listed in Table S1 (ESI†).

As can be seen in Fig. 3 it was possible to fabricate membranes with hexagonally ordered pores on the surface for all block copolymers. In general, two trends can be observed by comparing the surface structure in dependency of the molecular weight and the polymer concentration in the casting solution: (i) with increasing molecular weight, hexagonally ordered pores are achieved with decreasing polymer concentrations, (ii) with increasing molecular weight the pores get more and more inhomogeneous resulting in a larger pore size

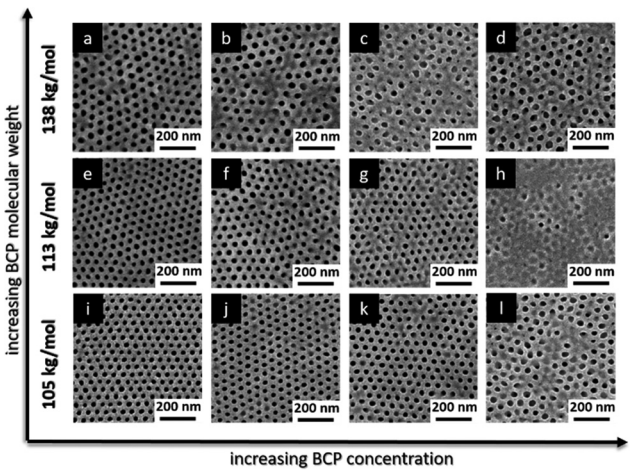


Fig. 3 SEM images of the membrane surfaces casted from PVBCB-*b*-P4VP block copolymers with varying molecular weights. The evaporation time prior to precipitation was varied. (a)–(d) Membranes were cast from PVBCB$_{80}$-*b*-P4VP$_{20}^{138k}$ block copolymer in DMF/THF/DIOX – 10/45/45 solutions with varying polymer concentrations between 14 and 18 wt%. (e)–(h) Membranes were cast from PVBCB$_{81}$-*b*-P4VP$_{19}^{113k}$ block copolymer in DMF/THF/DIOX – 10/45/45 solutions with varying polymer concentrations between 17 and 22 wt%. (i)–(l) Membranes were cast from PVBCB$_{80}$-*b*-P4VP$_{20}^{105k}$ block copolymer in DMF/THF/DIOX – 10/45/45 solutions with varying polymer concentrations between 18 and 24 wt%.

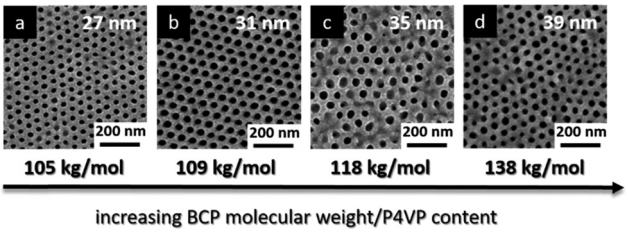


Fig. 4 SEM images of the membrane surfaces casted from PVBCB-*b*-P4VP block copolymers with increasing molecular weights resulting in enlarged pore diameters. (a) Membrane was cast from the $PVBCB_{80}$-*b*-$P4VP_{20}^{105k}$ block copolymer in DMF/THF/DIOX – 10/45/45 solution with a polymer concentration of 20 wt%. (b) Membrane was cast from the $PVBCB_{79}$-*b*-$P4VP_{21}^{109k}$ block copolymer in DMF/THF/DIOX – 10/45/45 solution with a polymer concentration of 20 wt%. (c) Membrane was cast from the $PVBCB_{79}$-*b*-$P4VP_{21}^{118k}$ block copolymer in DMF/THF/DIOX – 10/45/45 solution with a polymer concentration of 17 wt%. (d) Membrane was cast from the $PVBCB_{80}$-*b*-$P4VP_{20}^{138k}$ block copolymer in DMF/THF/DIOX – 10/45/45 solution with a polymer concentration of 14 wt%.

distribution. The PVBCB-*b*-P4VP block copolymers with molecular weights of 105 and 113 kg mol$^{-1}$ build perfectly hexagonally ordered pores on the surface while the block copolymer with the highest molecular weight of 138 kg mol$^{-1}$ shows more defects. In addition, the polymer concentration showing the best surface morphology is dramatically decreasing from 20 over 17 to 14 wt% when increasing the molecular weight of the block copolymers from 105 (Fig. 3j) over 113 (Fig. 3e) to 138 (Fig. 3a) kg mol$^{-1}$. These findings can both be explained by the structure formation process in solution during the evaporation time. On the one hand, longer polymer chains show a lower mobility in solution and are more hindered to self-assemble into uniform microphase separated structures within the given evaporation time resulting in more defects and larger pore size distributions. On the other hand, the molecular weight is the key parameter influencing the viscosity of the casting solution, which in turn affects the hydrodynamic properties of a micellar solution. In our polymer/solvent system, the diblock copolymers self-assemble into micelles, where the PVBCB segments build the corona and the P4VP block segments the core. During the evaporation time, the matrix building PVBCB segments start to precipitate while the pore forming P4VP segments are still swollen in DMF and equalize the shrinkage occurred by solidification of the matrix. This process requires a certain viscosity of the casting solution to generate perfect hexagonally ordered pores resulting in lower polymer concentrations with increasing molecular weights.

Furthermore, the molecular weights of the block copolymers have not only an effect on the pore distribution but also on the size of the resulting pores. For a deeper understanding, the surface structure of a series of block copolymers with different molecular weights were further investigated with respect to the resulting pore size. The best surface structures of the PVBCB-*b*-P4VP block copolymers with molecular weights of 105, 109, 118 and 138 kg mol$^{-1}$ are shown in Fig. 4. As already discussed above the best surface structure is achieved with decreasing polymer concentrations by increasing molecular weights. Fig. 4 shows a strong influence of the molecular weight on the resulting pore size. When increasing the molecular weight of the PVBCB-*b*-P4VP block copolymers from 105 over 109 and 118 to 138 kg mol$^{-1}$ the pore sizes are shifted from 27 over 31 and 35 to 39 nm. These results can also be explained by the micellar aggregation during the evaporation process. Block copolymers with higher molecular weights can self-assemble into larger micelles resulting in bigger pores after precipitation in water. But due to the increasing molecular weight the chain mobility in the solution is more hindered resulting in a larger pore size distribution and more inhomogeneous pores as already discussed above.

The corresponding parameters used for the membrane formation process by SNIPS resulting in the surfaces shown in Fig. 4 are summarized in Table 2. Additionally, the pore diameters and the molecular weights of the P4VP block segments of each block copolymer are listed.

To establish a direct correlation between the pore size and the molecular weight of the block copolymers the P4VP content

Table 2 Molecular characteristics of the PVBCB-*b*-P4VP block copolymers and casting conditions for membrane formation using the SNIPS process shown in Fig. 3

| | Polymer | $M_n$ [a] (kg mol$^{-1}$) | $M_{n,P4VP}$ [b] (kg mol$^{-1}$) | wt%/P4VP | $c_{BCP}$ (wt%) | DMF/THF/DIOX | $t_{evap.}$ (s) |
|---|---|---|---|---|---|---|---|
| a | $PVBCB_{80}$-*b*-$P4VP_{20}^{105k}$ | 105 | 21 | 20 | 18 | 45/10/45 | 17 |
| b | | | | | 20 | 45/10/45 | 17 |
| c | | | | | 22 | 45/10/45 | 17 |
| d | | | | | 24 | 45/10/45 | 11 |
| e | $PVBCB_{81}$-*b*-$P4VP_{19}^{113k}$ | 113 | 22 | 19 | 17 | 45/10/45 | 10 |
| f | | | | | 18 | 45/10/45 | 10 |
| g | | | | | 20 | 45/10/45 | 10 |
| h | | | | | 22 | 45/10/45 | 10 |
| i | $PVBCB_{80}$-*b*-$P4VP_{20}^{138k}$ | 138 | 28 | 20 | 14 | 45/10/45 | 10 |
| j | | | | | 16 | 45/10/45 | 10 |
| k | | | | | 17 | 45/10/45 | 10 |
| l | | | | | 18 | 45/10/45 | 5 |

[a] Molecular weight determined *via* a combination of SEC measurements and $^1$H NMR spectroscopy. [b] Molecular weight determined *via* $^1$H NMR spectroscopy.

should also be taken into account. The crucial factor at this point is the molecular weight of the different P4VP segments to compare the pore sizes because polymers with different molecular weights but different P4VP contents can have the same P4VP block lengths. In such a case, the corona of the micelles will be different, but the cores will have the same size leading to membrane surfaces with different PVBCB wall thickness but same pore size. If we also take the P4VP content into account the block copolymers PVBCB$_{80}$-*b*-P4VP$_{20}^{105k}$, PVBCB$_{80}$-*b*-P4VP$_{20}^{109k}$, PVBCB$_{79}$-*b*-P4VP$_{21}^{118k}$ and PVBCB$_{80}$-*b*-P4VP$_{20}^{138k}$ having P4VP blocks with molecular weights of 21, 23, 25 and 28 kg mol$^{-1}$. The average pore diameters are increasing linearly with the P4VP molecular weight from 27 to 39 nm. Consequently, the pore size of the membrane surface is predictable and can be tailor-made by simply adjusting the overall molecular weight of the block copolymer and the polymer composition of both block segments (Fig. S10, ESI†).

### Functionalization of PVBCB-*b*-P4BP block copolymer membranes

After the structure formation using the SNIPS process, the PVBCB-*b*-P4VP block copolymer membranes offer the opportunity for functionalization. The P4VP block segments possess a reactive site with the nitrogen in the pyridine ring that can be quaternized by alkyl halides. For this purpose, the PVBCB-*b*-P4VP membranes were placed in ethanol and after addition of octylbromide heated under reflux by varying the reaction time between 1 and 24 hours (Scheme 2).

The functionalization reaction of the PVBCB-*b*-P4VP block copolymer membranes resulting in pyridine quaternized membranes denoted as PVBCB-*b*-P4VPq. Due to the quaternization of the nitrogen the pyridine moieties get positively charged yielding in polyelectrolytes that are insoluble in organic solvents. Therefore, the membranes were characterized with respect to degree of functionalization *via* infrared spectroscopy (Fig. S9, ESI†). A cutout of the IR spectra in the range of 1350 to 1700 cm$^{-1}$ with all characteristic peaks is shown in Fig. 5.

The spectrum of the pristine PVBCB$_{81}$-*b*-P4VP$_{19}^{113k}$ block copolymer membrane (black curve) shows an intensive peak at a wavenumber of 1600 cm$^{-1}$ (blue lined box) indicating the existence of the tertiary amine group in the pyridine ring. In the case of the quaternized PVBCB-*b*-P4VPq membranes the peaks at a wavenumber of 1600 cm$^{-1}$ are decreasing while new peaks in the range between 1600–1650 cm$^{-1}$ (green lined box) are visible. These peaks can be assigned to the quaternized and positively charged nitrogen atoms in the pyridine moieties indicating the successful functionalization of the membranes. As can be seen in Fig. 5 the peaks at a wavenumber of 1600 cm$^{-1}$ are decreasing with increasing reaction time between 1 and 16 hours while the new peaks in the range of 1600–1650 cm$^{-1}$ are increasing showing the ongoing functionalization of the membranes. The spectra after 16 and 24 hours of functionalization are identical after integration of both peaks indicating complete quaternization after 16 hours of reaction.

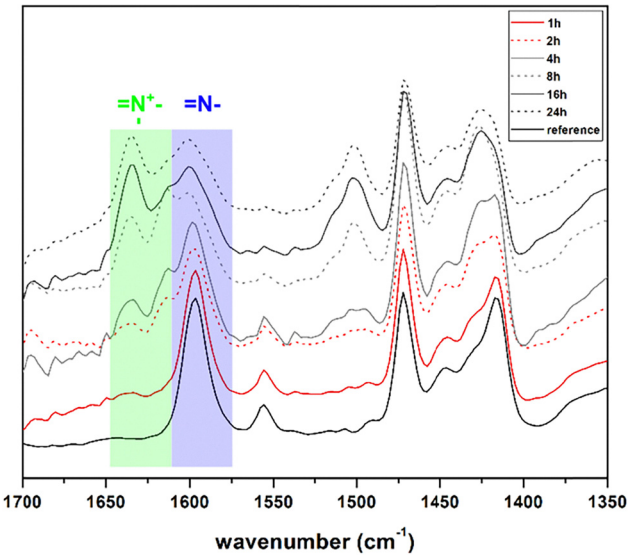


Fig. 5 Cutout of the IR spectra from functionalized PVBCB$_{81}$-*b*-P4VPq$_{19}^{113k}$ membranes in the range of 1350–1700 cm$^{-1}$. PVBCB$_{81}$-*b*-P4VPq$_{19}^{113k}$ membranes after 1 h (red line), 2 h (red dotted line), 4 h (grey line), 8 h (grey dotted line), 16 h (dark grey line) and 24 h (dark grey dotted line) of functionalization with octylbromide as well as the pristine PVBCB$_{81}$-*b*-P4VP$_{19}^{113k}$ membrane (black) are shown.

After the successful quaternization the PVBCB-*b*-P4VP block copolymer membranes were further investigated using SEM measurements with respect to their isoporous integral asymmetric structure. The surfaces of the pristine PVBCB$_{81}$-*b*-P4VP$_{19}^{113k}$ and quaternized PVBCB$_{81}$-*b*-P4VPq$_{19}^{113k}$ block copolymer membranes are shown in Fig. 6. As can be seen, the integral asymmetric structure is still alive after the reaction.

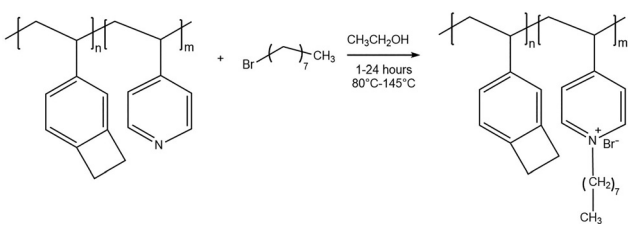


Scheme 2 Functionalization of the PVBCB-*b*-P4BP block copolymer membranes by quaternizing the pyridine moieties with octylbromide in ethanol under reflux.

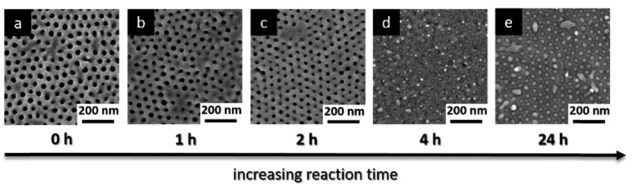


Fig. 6 SEM images of the PVBCB$_{81}$-*b*-P4VP$_{19}^{113k}$ and PVBCB$_{81}$-*b*-P4VPq$_{19}^{113k}$ block copolymers membrane surfaces. (a) Pristine non-functionalized PVBCB$_{81}$-*b*-P4VP$_{19}^{113k}$ membrane (b) PVBCB$_{81}$-*b*-P4VPq$_{19}^{113k}$ membrane after 1 h of functionalization. (c) PVBCB$_{81}$-*b*-P4VPq$_{19}^{113k}$ membrane after 2 h of functionalization. (d) PVBCB$_{81}$-*b*-P4VPq$_{19}^{113k}$ membrane after 4 h of functionalization. (e) PVBCB$_{81}$-*b*-P4VPq$_{19}^{113k}$ membrane after 24 h of functionalization.

The membranes are not soluble in ethanol and the glass transition temperatures with 125 and 145 °C are higher than the reaction temperature of 80 °C for which reason the membranes are stable under the reaction conditions and the structures is not affected. However, due to functionalization of the membranes with octylbromide the pores are getting smaller with increasing reaction time and start to close after 4 hours. As can be seen all pores are closed after a reaction time of 24 hours. This phenomenon can be explained by the underlying structure of the membrane surfaces. During the SNIPS process the block copolymers self-assemble to micelles and the P4VP block segments are forming the core. After a certain evaporation time and the precipitation of the membrane in a water bath the structure is frozen and the swollen P4VP core forming block segments are collapsing resulting in open cylindrical pores on the surfaces. Therefore, the membrane pores are consisting of P4VP, which are the segments that are functionalized with octylbromide, resulting in positively charged pores while the matrix forming PVBCB segments are not functionalized. With increasing reaction time, the degree of quaternization also increases as can be seen in the time dependent IR measurements. This effect leads to more positive charges and repulsion forces inside the membrane pores resulting in stretching of the polymer chains leading to smaller pores and the complete closure after 4 hours of functionalization. Nevertheless, the PVBCB-*b*-P4VP block copolymer membranes can be easily functionalized with alkylhalides in refluxing ethanol by simply optimizing the reaction time.

### Flux and retention measurements

The control of the pore size and high porosity as well as the functionalization of these membranes making them to ideal candidates for size selective separation processes. Next to uniform pores on the surface also an asymmetric membrane structure with a highly porous sponge-like supporting layer is very important for selective and fast filtration processes. Exemplarily the cross-section of the $PVBCB_{80}$-*b*-$P4VP_{20}^{105k}$ block copolymer membrane is shown in Fig. 7. As can be seen, the membrane possesses hexagonally ordered pores on the surface and a porous sponge like supporting layer resulting in an isoporous integral asymmetric membrane. In contrast to other known block copolymer membranes made from PS-*b*-P4VP the new PVBCB-*b*-P4VP membranes show a homogenous three-dimensional porosity throughout the whole body of the material like polymeric foams. The new PVBCB-*b*-P4VP membranes developed in this study combine the characteristics of the three-dimensional porosity of polymer foams with the surface selective layer of flat sheet membranes.

Table 3 Comparison of water flux of PVBCB-*b*-P4VP and PS-*b*-P4VP block copolymer membranes depending on the pore diameter

| | Polymer | $d_{pore}$[a] (nm) | Water flux (L $h^{-1}$ × $m^{-2}$ $bar^{-1}$) |
|---|---|---|---|
| a | $PVBCB_{80}$-*b*-$P4VP_{20}^{105k}$ | 27 | 22 |
| b | $PVBCB_{79}$-*b*-$P4VP_{21}^{109k}$ | 31 | 158 |
| c | $PS_{75}$-*b*-$P4VP_{25}^{100k}$ | 25 | 450 |
| d | $PS_{74}$-*b*-$P4VP_{26}^{160k}$ | 38 | 625 |

[a] Pore size of membranes was determined by SEM measurements.

To check the performance of the membranes time-dependent water flux measurements were carried out in dead-end mode at room temperature showing low but constant water flux. The membranes having pore diameters of 27 and 31 nm showing permeances of 22 and 158 L $h^{-1}$ $m^{-2}$ $bar^{-1}$. In Table 3 the pore diameters and experimental flux values are shown as well as flux values from the literature for PS-*b*-P4VP block copolymer membranes having similar pore diameters. Compared to the flux values of PS-*b*-P4VP membranes from the literature,[9] the new PVBCB-*b*-P4VP membranes developed in the study show minor water flux. These findings are attributed to the three-dimensional porosity of the substructure. Usually, the isoporous block copolymer membrane support layer is dominated by cavities with holes that are much larger than the average pore size of the pores so that the separation takes

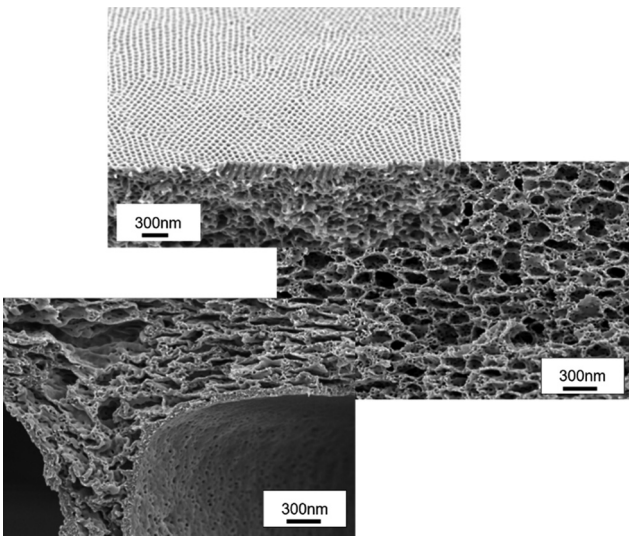


Fig. 7 SEM images of the cross-section of $PVBCB_{80}$-*b*-$P4VP_{20}^{105k}$ block copolymer membrane showing the isoporous integral asymmetric structure.

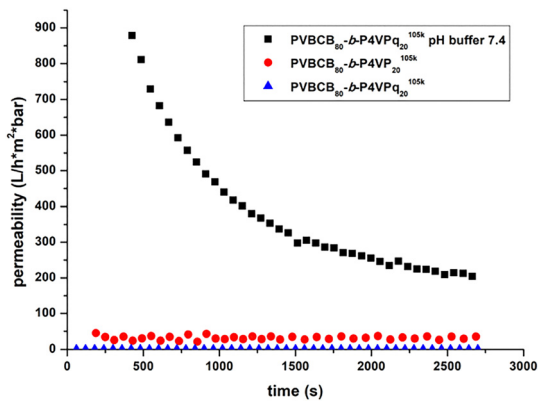


Fig. 8 Water flux measurements of block copolymer membranes $PVBCB_{80}$-*b*-$P4VP_{20}^{105k}$, $PVBCB_{80}$-*b*-$P4VPq_{20}^{105k}$ and $PVBCB_{80}$-*b*-$P4VPq_{20}^{105k}$ in PBS buffer with pH of 7.4.

Table 4 Comparison of water flux, pore diameter as well as BSA and Hb retention of PVBCB-*b*-P4VP, PVBCB-*b*-P4VPq and PS-*b*-P4VP block copolymer membranes depending on pore diameter

| | Polymer | $d_{pore}$ (nm)[a] | Water flux (L $h^{-1}$ $m^{-2}$ $bar^{-1}$) | % BSA retention | % Hb retention |
|---|---|---|---|---|---|
| a | $PVBCB_{80}$-*b*-$P4VP_{20}^{105k}$ | 27 | 22 | 95 | 98 |
| b | $PVBCB_{80}$-*b*-$P4VPq_{20}^{105k}$ | 27 | 200 | 80 | 86 |
| d | $PS_{84}$-*b*-$P4VP_{16}^{113k}$ | 23 | 50 | 90 | — |

[a] Pore size of membranes was determined by SEM measurements.

place only on the membrane top layer. In this case, the existing cavities have the same porosity as the selective layer so that the separation occurs not only on the top layer but also in between the membranes.

Additionally, the performance of the quaternized membranes was tested by time-dependent water flux measurements in dead-end mode at room temperature. The flux measurements of the pristine $PVBCB_{80}$-*b*-$P4VP_{20}^{105k}$ and quaternized $PVBCB_{80}$-*b*-$P4VPq_{20}^{105k}$ membranes are shown in Fig. 8. As can be seen the flux is decreased after the functionalization of the block copolymer membrane (red dotted line-pristine membrane, blue triangle line-P4VP functionalized membrane). Due to the functionalization reaction, the P4VP block segments get quaternized resulting in positively charged pores. Therefore, the pores start to swell like a polyelectrolyte when coming in contact with water leading to smaller pore diameters and consequently to a lower/non-water flux (blue triangle line). But as the water flux for both membranes were measured in a PBS buffer at pH 7.4, the water flux of the functionalized membrane increased dramatically from 0 to 200 L $h^{-1}$ $m^{-2}$ $bar^{-1}$. It appears that the pores are not able to swell in the buffer solution and due to the positive charged pores, the high polarity allows an increased water flux for the functionalized membranes while the flux of the pristine membrane is not affected by the buffer solution.

Furthermore, the separation properties of the membranes were tested by protein retention measurements. For this purpose, BSA and hemoglobin (Hb) were dissolved in PBS buffer solution at a concentration of 1 g $L^{-1}$, each. The membrane with a pore diameter of *xy* nm showing BSA and Hb retention of 95 and 98% (Table 4). Compared to the retention of PS-*b*-P4VP membranes with similar pore sizes from the literature the new developed PVBCB-*b*-P4VP membranes in the study showing a significant higher retention of proteins. This improved retention can be again assigned to the three-dimensional porosity of the membrane body. On the one hand, this foam-like substructure results in a lower water flux but on the other hand, an improved protein retention can be observed.

In a last step, the retention properties of the quaternized membranes were also tested. In this case, retention measurements of the pristine $PVBCB_{80}$-*b*-$P4VP_{20}^{105k}$ and quaternized $PVBCB_{80}$-*b*-$P4VPq_{20}^{105k}$ membranes were carried out for BSA and Hb (see Table 4). The quaternized membrane shows a decreased retention of BSA and Hb in contrast to the pristine membrane, which can be explained by the ten times higher flux and the positively charged pores. But in general, it was shown that it's possible to introduce positive charge into the pyridine moieties resulting in a smart and switchable membrane.

## Conclusions

We showed the membrane formation of new PVBCB-*b*-P4VP block copolymers resulting in an isoporous integral asymmetric structure comprising a unique foam-like substructure with a homogenous three-dimensional porosity throughout the whole membrane body. The block copolymers were synthesized by sequential anionic polymerization and were characterized with respect to their molecular weights, compositions and thermal properties using SEC, $^1$H-NMR spectroscopy and DSC measurements. The membranes were fabricated *via* combination of the self-assembly of the block copolymers and the non-solvent induced phase separation process resulting in isoporous integral asymmetric membranes. Structure formation using SNIPS process depends on the evaporation time, the polymer concentration of the initial casting solution and the molecular weight as well as the block copolymer composition was investigated. It was shown that structure formation with increasing molecular weight of the block copolymers takes place by decreasing polymer concentrations of the initial casting solution. The membrane surfaces and cross-sections were characterized by SEM measurements in order to determine the structure building process. Furthermore, the linear dependency of the pore diameters from the molecular weight of the pore forming P4VP block segments was shown. In this regard, the pore diameters were tailor-made in the range of 26 to 38 nm by simply adjusting the molecular weight of the P4VP block segments between 19 and 27 kg $mol^{-1}$.

In a second step, the fabricated membranes were functionalized with octylbromide in a post-functionalization reaction in ethanol. Due to the functionalization the P4VP block segments were quaternized resulting in membranes with positively charged pores which were confirmed by IR spectroscopy. The quaternized PVBCB-*b*-P4VPq BCP membranes were characterized by SEM measurements with respect to their surface structures. It was shown that the pores were getting smaller with an increasing degree of functionalization and started to close after 4 hours of functionalization. Moreover, the performance of the pristine and the quaternized membranes was tested by time-dependent water flux and retention measurements in dead-end mode at room temperature. PVBCB-*b*-P4VP block copolymers revealed a lower water permeance but significant higher protein retention than the well-studied PS-*b*-P4VP block copolymer membranes. In this regard, SEM measurements of the cross-section showed that the new membranes consisting of a thin selective layer like flat sheet membranes and a substructure with a homogenous three-dimensional porosity throughout the whole membrane body like a polymeric foam. Due to this unique foam-like substructure the new PVBCB-*b*-P4VP block copolymer membranes show lower permeability but higher selectivity than consisting of

PS-*b*-P4VP membranes. Furthermore, the quaternized PVBCB-*b*-P4VP block copolymer membranes showed lower water flux than non-functionalized membranes due to the swelling of the positively charged pores in water. Finally, the functionalized membranes showed much higher retention of positively charged dyes in contrast to the non-quaternized membranes because of the electrostatic repulsion of the positive charges.

## Author contributions

The manuscript was written through contributions of all authors. All authors have given approval to the final version of the manuscript.

## Conflicts of interest

There are no conflicts to declare.

## Data availability

The data supporting this article have been included as part of the ESI.†

## Acknowledgements

The authors acknowledge the Helmholtz community (technology transfer project CROSSIMEM) for financial support of this work. The authors thank Barbara Bajer, Petra Merten, Silvio Neumann, Maren Brinkmann, Martin Held, Erik Schneider and Anke-Lisa Höhme for their help with NMR, SEC, water flux and SEM measurements as well as retention experiments.

## References

1 B. Bruggen, 2017, DOI: 10.1002/0471238961.1305130202011105.a01.pub3.
2 S. P. Nunes, *Macromolecules*, 2016, **49**, 2905–2916.
3 D. M. Alshangiti, T. K. El-Damhougy, A. Zaher, M. Madani and M. Mohamady Ghobashy, *RSC Adv.*, 2023, **13**, 35251–35291.
4 Y. Gao, S. Wang, B. Shi, Y. Wang, Y. Chen, X. Wang, E. S. Lee and H. B. Jiang, *Polymers*, 2022, **14**, 4804.
5 X. Hu, T. Wang, F. Li and X. Mao, *RSC Adv.*, 2023, **13**, 20495–20511.
6 M. Hren, M. Božič, D. Fakin, K. S. Kleinschek and S. Gorgieva, *Sustainable Energy Fuels*, 2021, **5**, 604–637.
7 C. Astorino, E. De Nardo, S. Lettieri, G. Ferraro, C. F. Pirri and S. Bocchini, *Membranes*, 2023, **13**, 903.
8 Y. Mai and A. Eisenberg, *Chem. Soc. Rev.*, 2012, **41**, 5969–5985.
9 S. Rangou, K. Buhr, V. Filiz, J. I. Clodt, B. Lademann, J. Hahn, A. Jung and V. Abetz, *J. Membr. Sci.*, 2014, **451**, 266–275.
10 F. S. Bates, M. A. Hillmyer, T. P. Lodge, C. M. Bates, K. T. Delaney and G. H. Fredrickson, *Science*, 2012, **336**, 434–440.
11 X.-Q. Wang, T. Wang, Y.-N. Feng, L.-Y. Zhang and Z.-P. Zhao, *Sustainable Mater. Technol.*, 2024, **39**, e00855.
12 M. Radjabian and V. Abetz, *Adv. Mater.*, 2015, **27**, 352–355.
13 S. P. Nunes, A. R. Behzad, B. Hooghan, R. Sougrat, M. Karunakaran, N. Pradeep, U. Vainio and K.-V. Peinemann, *ACS Nano*, 2011, **5**, 3516–3522.
14 A. Jung, V. Filiz, S. Rangou, K. Buhr, P. Merten, J. Hahn, J. Clodt, C. Abetz and V. Abetz, *Macromol. Rapid Commun.*, 2013, **34**, 610–615.
15 V. Abetz, *Macromol. Rapid Commun.*, 2015, **36**, 10–22.
16 S. Saleem, S. Rangou, C. Abetz, V. Filiz and V. Abetz, *Polymers*, 2020, **12**, 41.
17 J. Hahn, J. I. Clodt, V. Filiz and V. Abetz, *RSC Adv.*, 2014, **4**, 10252–10260.
18 J. Hahn, V. Filiz, S. Rangou, B. Lademann, K. Buhr, J. I. Clodt, A. Jung, C. Abetz and V. Abetz, *Macromol. Mater. Eng.*, 2013, **298**, 1315–1321.
19 S. Rangou, M. Appold, B. Lademann, K. Buhr and V. Filiz, *ACS Macro Lett.*, 2022, **11**, 1142–1147.